Journal of Nuclear Medicine, published on November 16, 2023 as doi:10.2967/jnumed.123.266148

Imaging of Myocardial $\alpha_v\beta_3$ Integrin Expression for Evaluation of Myocardial Injury After Acute Myocardial Infarction

Wail Nammas*[1,2], Christian Paunonen*[1], Jarmo Teuho[1], Reetta Siekkinen[1,3], Pauliina Luoto[1], Meeri Käkelä[1], Ari Hietanen[1], Tapio Viljanen[1], Matthieu Dietz[4], John O. Prior[4], Xiang-Guo Li[1,5,6], Anne Roivainen[1,6], Juhani Knuuti[1,6], and Antti Saraste[1,2,6]

[1]*Turku PET Centre, Turku University Hospital and University of Turku, Turku, Finland;* [2]*Heart Center, Turku University Hospital, University of Turku, Turku, Finland;* [3]*Department of Medical Physics, Turku University Hospital, Turku, Finland;* [4]*Department of Nuclear Medicine and Molecular Imaging, Lausanne University Hospital, Lausanne, Switzerland;* [5]*Department of Chemistry, University of Turku, Turku, Finland; and* [6]*InFLAMES Research Flagship Center, University of Turku, Turku, Finland*

[^{68}Ga]Ga-NODAGA-Arg-Gly-Asp (RGD) is a PET tracer targeting $\alpha_v\beta_3$ integrin, which is upregulated during angiogenesis soon after acute myocardial infarction (AMI). We prospectively evaluated determinants of myocardial uptake of [^{68}Ga]Ga-NODAGA-RGD and its associations with left ventricular (LV) function in patients after AMI. **Methods:** Myocardial blood flow and [^{68}Ga]Ga-NODAGA-RGD uptake (60 min after injection) were evaluated by PET in 31 patients 7.7 ± 3.8 d after primary percutaneous coronary intervention for ST-elevation AMI. Transthoracic echocardiography of LV function was performed on the day of PET and at the 6-mo follow-up. **Results:** PET images showed increased uptake of [^{68}Ga]Ga-NODAGA-RGD in the ischemic area at risk (AAR), predominantly in injured myocardial segments. The SUV in the segment with the highest uptake (SUV_{max}) in the ischemic AAR was higher than the SUV_{mean} of the remote myocardium (0.73 ± 0.16 vs. 0.51 ± 0.11, $P < 0.001$). Multivariable predictors of [^{68}Ga]Ga-NODAGA-RGD uptake in the AAR included high peak N-terminal pro–B-type natriuretic peptide ($P < 0.001$), low LV ejection fraction, low global longitudinal strain ($P = 0.01$), and low longitudinal strain in the AAR ($P = 0.01$). [^{68}Ga]Ga-NODAGA-RGD uptake corrected for myocardial blood flow and perfusable tissue fraction in the AAR predicted improvement in global longitudinal strain at follow-up ($P = 0.002$), independent of peak troponin, N-terminal pro–B-type natriuretic peptide, and LV ejection fraction. **Conclusion:** [^{68}Ga]Ga-NODAGA-RGD uptake shows increased $\alpha_v\beta_3$ integrin expression in the ischemic AAR early after AMI that is associated with regional and global systolic dysfunction, as well as increased LV filling pressure. Increased [^{68}Ga]Ga-NODAGA-RGD uptake predicts improvement of global LV function 6 mo after AMI.

Key Words: myocardial infarction; PET; angiogenesis; myocardial strain; coronary artery disease

J Nucl Med 2024; 00:1–7
DOI: 10.2967/jnumed.123.266148

Acute myocardial infarction (AMI) initiates maladaptive changes in cardiac myocytes and the extracellular matrix, which can contribute to left ventricular (LV) dysfunction, adverse remodeling, and eventual failure (*1*). The repair process aimed at restoration of the capillary network, elimination of necrotic tissue, and deposition of new extracellular matrix is essential for healing of AMI and can counteract the development of chronic LV dysfunction (*1*). In parallel with inflammation and fibrosis, angiogenesis (sprouting of preexisting capillaries) plays an important role in myocardial repair after AMI (*2*).

Integrin $\alpha_v\beta_3$ is a glycoprotein transmembrane receptor the expression of which is upregulated in proliferating endothelial cells and can serve as a biomarker of angiogenesis (*3*). After AMI, $\alpha_v\beta_3$ integrin expression increases in vascular structures during the early repair process (*4*). Studies in experimental models and humans demonstrated the feasibility of using radiolabeled tracers containing the Arg-Gly-Asp (RGD) motif for the noninvasive detection of $\alpha_v\beta_3$ integrin expression after AMI (*5–13*). However, the clinical utility of $\alpha_v\beta_3$ integrin as a biomarker after AMI remains uncertain.

We sought to study the determinants of $\alpha_v\beta_3$ integrin expression and its association with LV function after AMI. We prospectively evaluated myocardial uptake of [^{68}Ga]Ga-NODAGA-RGD (*10,14*), a PET radiotracer targeting $\alpha_v\beta_3$ integrin, within 2 wk of reperfusion in patients with AMI. The function of the LV was evaluated by echocardiography at the time of the PET scan and 6 mo later.

MATERIALS AND METHODS

Study Cohort and Design

We prospectively recruited patients who underwent primary percutaneous coronary intervention because of ST-elevation AMI and who had an LV ejection fraction (LVEF) of less than 50% during the index hospitalization in Turku University Hospital from December 2018 to January 2021. Exclusion criteria are listed in the supplemental materials (available at http://jnm.snmjournals.org). Each patient signed an informed consent form. The study conforms to the Declaration of Helsinki, and the institutional review boards of the Hospital District of Southwest Finland, Finnish Medicines Agency, and Turku University Hospital approved the study. The study was registered in clinicaltrials.gov with identifier NCT04871217.

To evaluate myocardial $\alpha_v\beta_3$ integrin expression, patients underwent [^{15}O]O-water PET followed by [^{68}Ga]Ga-NODAGA-RGD PET within 3 to 14 d after AMI. To evaluate LV function, echocardiography was performed at baseline on the day of PET imaging and at the 6-mo follow-up. Peak cardiac troponin T and N-terminal pro–B-type natriuretic peptide (NT-proBNP) levels were recorded during hospitalization and at the time of PET imaging. Data on cardiovascular risk factors, medications, and cardiovascular events were collected from

Received Jun. 8, 2023; revision accepted Sep. 27, 2023.
For correspondence or reprints, contact Antti Saraste (antti.saraste@utu.fi).
*Contributed equally to this work.
Published online Nov. 16, 2023.

electronic medical reports. The myocardial area at risk (AAR) and the remote area were based on the culprit coronary arterial segment, determined from the invasive coronary angiography and electrocardiography.

PET Imaging

Synthesis of [^{68}Ga]Ga-NODAGA-RGD is described in the supplemental materials. For each patient, resting [^{15}O]O-water and [^{68}Ga]Ga-NODAGA-RGD PET scans were performed using a dedicated PET/CT scanner (Discovery MI; GE Healthcare) on the same day, as previously described (supplemental materials) (*15*). In brief, [^{15}O]O-water (Radiowater Generator; Hidex Oy) was injected as an intravenous bolus (target injected radioactivity, 500 MBq) over 15 s, and dynamic PET was performed over 4 min and 40 s, starting 25 s after injection, with the patient at rest. Then, an average of 179 ± 15 MBq of [^{68}Ga]Ga-NODAGA-RGD was injected as an intravenous bolus and was followed by a list-mode PET acquisition over 15 min after a 60-min uptake period.

PET Image Analysis and Interpretation

Images were analyzed using Carimas 2.9 software (Turku PET Centre) (supplemental materials) (*10,16*). In brief, polar maps of [^{68}Ga]Ga-NODAGA-RGD uptake (SUV) in the LV myocardium were based on myocardial contours and sampling points matching with coregistered [^{15}O]O-water images. The [^{68}Ga]Ga-NODAGA-RGD SUV_{max} was defined as the highest segmental uptake. An indexed SUV_{max} corrected for the mean myocardial blood flow (MBF) and perfusable tissue fraction in the AAR was also calculated to account for the reduced amount of viable tissue in the infarct zone (*16*).

Echocardiography

Transthoracic echocardiography was performed using Vivid E9 or E95 (GE Vingmed Ultrasound) devices equipped with MS5 and 4Vc-D 4-dimensional probes. All images were digitally stored for offline analysis (EchoPAC PC version 203; GE Vingmed) of LV global and segmental function (supplemental materials). The LV volumes and LVEF were measured using the biplane Simpson method. Myocardial global longitudinal strain (GLS) and segmental longitudinal strain (LS) were analyzed using the speckle-tracking method and reported as absolute values. Segments with a baseline LS of less than 13.5% were defined as injured (*17*).

Statistical Analysis

Continuous data are reported as mean and SD and compared using the Student *t* test when normally distributed or with the Mann–Whitney test otherwise. Categoric data are reported as count and percentage and compared with χ^2 or Fisher exact tests, as appropriate. Univariable and multivariable linear regression models were constructed to identify predictors of [^{68}Ga]Ga-NODAGA-RGD uptake at baseline and predictors of improvement in LV function from baseline to follow-up. Statistically significant variables in the univariable analysis were added to multivariable models as covariates. Intra- and interobserver reproducibility of [^{68}Ga]Ga-NODAGA-RGD SUV_{max} measures were assessed in 7 randomly selected patients by calculating the coefficient of variation. Statistical significance was set at a *P* value of less than 0.05. Statistical analyses were performed using SPSS version 25.0 (IBM Corp.).

RESULTS

We enrolled 31 patients with the first ST-elevation AMI. Table 1 summarizes the baseline characteristics of the patients. All patients underwent primary percutaneous coronary intervention at 4.9 ± 6.1 h from symptom onset. The AAR was in the left anterior descending, the right, and the left circumflex coronary artery territories in 48.4%, 29.0%, and 22.6% of patients, respectively.

TABLE 1
Patient Characteristics (*n* = 31)

Characteristic	Data
Age (y)	64.2 ± 9.2
Male sex	28 (90.3%)
Body mass index (kg/m^2)	25.4 ± 4.8
Current smoking	11 (35.5%)
Diabetes mellitus	3 (9.7%)
Hypertension	13 (41.9%)
Hypercholesterolemia	17 (54.8%)
Family history of CAD	9 (31%)
Time from symptoms to PCI (h)	4.9 ± 6.1
Culprit coronary artery territory	
Left anterior descending artery	15 (48.4%)
Circumflex artery	7 (22.6%)
Right coronary artery	9 (29%)
Post-PCI TIMI flow	
Grade 2	10 (32.3%)
Grade 3	21 (67.7%)
Peak troponin T (ng/L)	3884.3 ± 4391.7
Peak NT-proBNP (ng/L)	979.4 ± 871.5
Total cholesterol (mmol/L)	4.2 ± 1.1
LDL cholesterol (mmol/L)	2.9 ± 0.9
Duration of hospital stay (d)	3.7 ± 1.8
Loop diuretics	10 (32.3%)
Inotropic medication	7 (22.6%)
Medication at discharge	
Aspirin	30 (96.8%)
Statin	30 (96.8%)*
ACEI/ARB	29 (93.5%)
β-blocker	25 (80.6%)

*High-intensity statin in 27 (87.1%).

CAD = coronary artery disease; PCI = percutaneous coronary intervention; TIMI = thrombolysis in myocardial infarction; LDL = low-density lipoprotein; ACEI/ARB = angiotensin-converting enzyme inhibitor/angiotensin receptor blocker.

Qualitative data are number and percentage; continuous data are mean ± SD.

Patients underwent [^{15}O]O-water and [^{68}Ga]Ga-NODAGA-RGD PET scans at 7.7 ± 3.8 d (median, 8 d; interquartile range, 7 d) after AMI. The clinical characteristics were similar between patients who underwent PET at less than 7 d after AMI (*n* = 14) and patients who underwent PET at 7 d or more after AMI (*n* = 17).

One patient was lost to follow-up. Consequently, 30 patients underwent both baseline and follow-up echocardiography 210 ± 38 d after AMI. There were no deaths or heart failure hospitalizations during follow-up, but 1 patient had non–ST-elevation AMI caused by a coronary lesion other than the index lesion.

LV Function

Table 2 summarizes the echocardiography data. All patients initially had an LVEF of less than 50%, whereas at baseline evaluation

TABLE 2
Echocardiography Data

Parameter	Baseline (n = 31)	Follow-up (n = 30)	P
LV end-diastolic volume (mL)	94.7 ± 27.7	93.6 ± 30.1	0.7
LV end-systolic volume (mL)	42.7 ± 17.1	40.8 ± 19.1	0.4
LVEF (%)	55.8 ± 6.9	57.5 ± 7.3	0.2
GLS (%)	14.9 ± 4.6	15.4 ± 3.9	0.3
LS in AAR (%)	12.5 ± 6.0	13.8 ± 5.2	0.03
Mitral E/A ratio	0.96 ± 0.35	1.01 ± 0.36	0.4
E/e′ ratio	8.9 ± 2.7	7.7 ± 1.8	0.01

E/A = early diastolic filling velocity/atrial filling velocity; E/e′ = early diastolic filling velocity/early diastolic tissue velocity.
Data are mean ± SD.

on the day of PET scanning, LVEF was less than 50% in 5 patients and GLS was less than 16% in 17. In the AAR, myocardial injury (segmental LS < 13.5%) was present in 26 (84%) patients. The average number of injured segments per patient was 3.1 ± 2.2.

At follow-up, LS in the AAR showed significant improvement from baseline (P = 0.03). LVEF improved by at least 5% in 12 (40%) patients and worsened by at least 5% in 6 (20%). In turn, GLS improved by at least 3% in 9 (30%) patients and worsened by at least 3% in 4 (13%). Only 4 patients had an LV end-diastolic volume increase of at least 20%.

[^{68}Ga]Ga-NODAGA-RGD Uptake After AMI

Uptake of [^{68}Ga]Ga-NODAGA-RGD was visible in the AAR in PET images from all patients (Fig. 1; Supplemental Fig. 1). The segment with the highest [^{68}Ga]Ga-NODAGA-RGD uptake (SUV_{max}) was within or immediately adjacent to the AAR in all patients. Segments in the AAR (n = 168) showed higher [^{68}Ga]Ga-NODAGA-RGD SUV than segments in the remote area (0.66 ± 0.18 vs. 0.55 ± 0.14, P < 0.001, Fig. 2).

The [^{68}Ga]Ga-NODAGA-RGD SUV_{max} colocalized with the segment with the most severe contractile abnormality or the immediately adjacent segment in 22 patients. In the remaining patients, SUV_{max} was either in the border of a large injured area (n = 4) or there was no contractile abnormality in the AAR (n = 5). Within the AAR, the average [^{68}Ga]Ga-NODAGA-RGD SUV was higher in segments with myocardial injury (n = 97) than in other segments (0.71 ± 0.19 vs. 0.61 ± 0.14, P < 0.001, Fig. 2) and inversely correlated with LS (P < 0.001, Fig. 3A).

MBF was lower in the AAR than in remote myocardium (0.73 ± 0.23 vs. 0.83 ± 0.23 mL/g/min, P < 0.001). There was no correlation between segmental SUV and overall MBF in the AAR (P = 0.1), but SUV_{max} correlated with MBF in the non-injured myocardial segments within or immediately adjacent to AAR (r = 0.49, P = 0.017, Supplemental Fig. 2).

In patient-based analysis, SUV_{max} and indexed SUV_{max} were higher in the AAR than in remote myocardium (Table 3). SUV_{max} in the AAR was higher than blood pool SUV (0.73 ± 0.16 vs. 0.64 ± 0.15, P < 0.001) but lower than liver SUV (0.73 ± 0.16 vs. 1.04 ± 0.16, P < 0.001). SUV_{max} was similar between patients who underwent PET at less than 7 d after AMI and patients who underwent PET at 7 d or more after AMI (P > 0.05, Supplemental Table).

Measurement of SUV_{max} was reproducible, with an intraobserver coefficient of variation of 1.4% and an interobserver coefficient of variation of 10.9%.

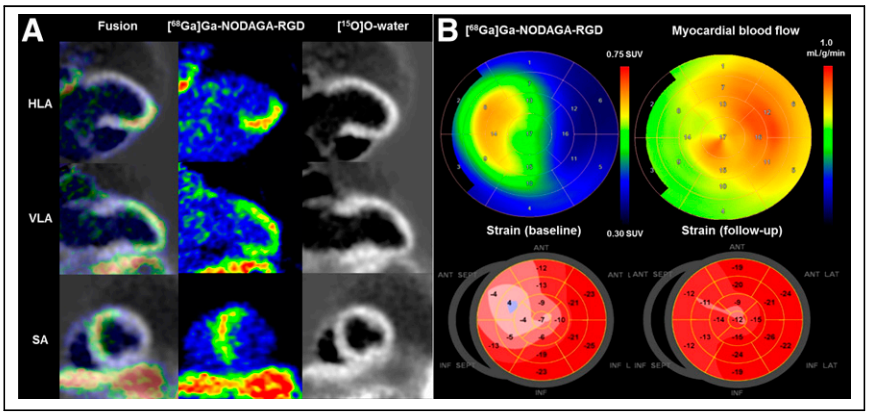

FIGURE 1. Uptake of [^{68}Ga]Ga-NODAGA-RGD 7 d after acute occlusion of proximal left anterior descending coronary artery. (A) Myocardial contours in [^{15}O]O-water images, [^{68}Ga]Ga-NODAGA-RGD uptake images, and corresponding fusion images. (B) Polar maps of [^{68}Ga]Ga-NODAGA-RGD uptake, resting MBF, and longitudinal strain at time of PET and 6 mo later. Reduced longitudinal strain is seen in anteroseptal region at baseline and partial functional recovery at 6 mo. HLA = horizontal long axis; SA = short axis; VLA = vertical long axis.

Predictors of [^{68}Ga]Ga-NODAGA-RGD Uptake After AMI

Univariable predictors of [^{68}Ga]Ga-NODAGA-RGD SUV_{max} and indexed SUV_{max} in the AAR at baseline included peak troponin T, peak NT-proBNP, GLS, and LS in the AAR (Table 4). Neither age nor peak CRP level predicted SUV_{max} or indexed SUV_{max} (P > 0.05 for both), which were similar in patients with postrevascularization thrombolysis in myocardial infarction flow grade 2 or 3 (P = 0.6).

In multivariable models, the only independent predictor of SUV_{max} in the AAR was peak NT-proBNP (Fig. 3B; Table 4), whereas peak troponin T, LVEF, and GLS predicted indexed SUV_{max} (Table 4).

[^{68}Ga]Ga-NODAGA-RGD Uptake and LV Function at Follow-up

In univariable analysis, indexed [^{68}Ga]Ga-NODAGA-RGD SUV_{max} in the AAR, peak

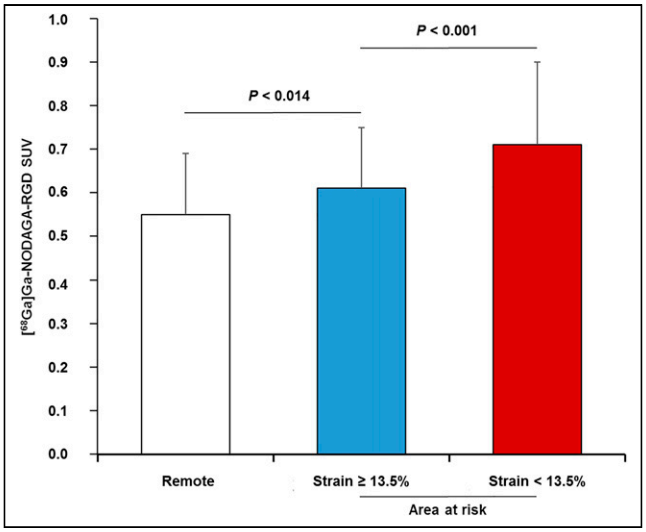

FIGURE 2. At baseline, segmental uptake of [^{68}Ga]Ga-NODAGA-RGD was higher in AAR than in remote myocardium and was highest in segments with myocardial injury (longitudinal strain < 13.5%).

troponin T, peak NT-proBNP, and baseline LVEF predicted improvement of GLS adjusted for baseline (Table 5). Neither time from symptom onset to revascularization nor the postrevascularization thrombolysis in myocardial infarction flow grade predicted improvement of GLS. In multivariable analysis, indexed SUV_{max} in the AAR was the only independent predictor of improvement of GLS at follow-up ($P = 0.002$, Fig. 4).

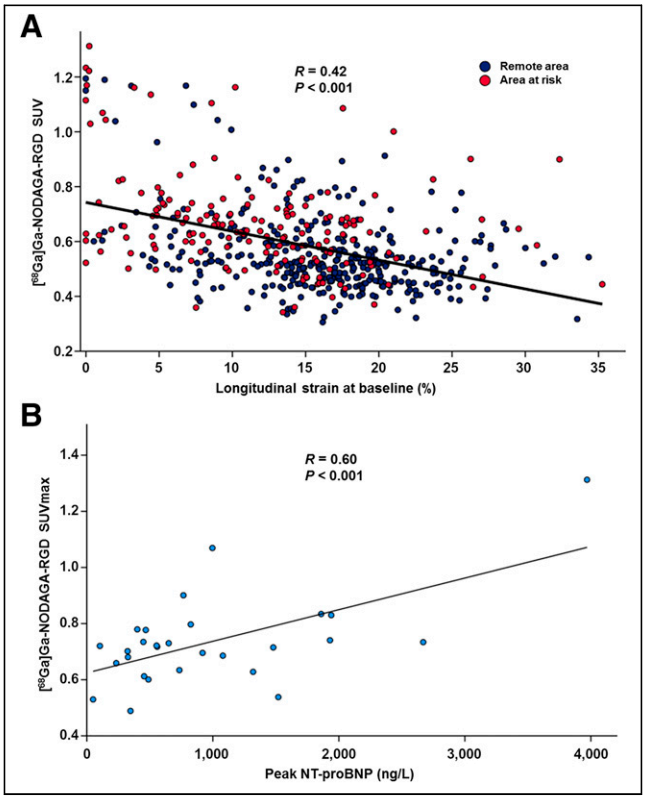

FIGURE 3. (A) Segmental uptake of [^{68}Ga]Ga-NODAGA-RGD inversely correlated with LS ($r = -0.0355$, $P < 0.001$). (B) Increased NT-pro-BNP level predicted [^{68}Ga]Ga-NODAGA-RGD SUV_{max} in AAR ($P < 0.001$).

Although associated with global LV function improvement, indexed SUV_{max} was not associated with improvement of LS in the AAR in 26 patients with myocardial injury at baseline ($P = 0.7$). Furthermore, segmental [^{68}Ga]Ga-NODAGA-RGD SUV did not correlate with change in LS in injured segments in the AAR ($P = 0.2$).

DISCUSSION

We found that uptake of [^{68}Ga]Ga-NODAGA-RGD increased in the myocardium distal to the culprit lesion of the infarct-related artery (AAR) in patients with recent ST-elevation AMI. Uptake of [^{68}Ga]Ga-NODAGA-RGD was associated with myocardial injury, regional and global LV systolic dysfunction, and increased LV filling pressure. Furthermore, the intensity of [^{68}Ga]Ga-NODAGA-RGD uptake was associated with improvement in global LV function at the 6-mo follow-up. These results indicate that [^{68}Ga]Ga-NODAGA-RGD PET provides information about the severity of acute ischemic myocardial injury and the potential for recovery of LV function.

Earlier studies demonstrated the feasibility of noninvasive nuclear imaging of $\alpha_v\beta_3$ integrin expression using radiolabeled tracers containing the RGD motif after recent AMI (*5–13*). Early after AMI, $\alpha_v\beta_3$ integrin is expressed by vascular endothelial cells (*4*), and uptake of RGD-based tracers correlates with neovascularization (*5–13*). However, $\alpha_v\beta_3$ integrin has also been implicated in mediating the macrophage response to inflammatory signals (*18*) and myofibroblast differentiation through the activation of transforming growth factor β1 (*19*), which may be also targeted by RGD-based tracers late after AMI (*20*). Thus, $\alpha_v\beta_3$ integrin expression may provide information about the activation of the repair process after ischemic myocardial injury, but its utility as an imaging biomarker after human AMI remains uncertain.

Uptake of [^{68}Ga]Ga-NODAGA-RGD After Myocardial Infarction

^{68}Ga-RGD tracers were previously demonstrated to accumulate in areas of injured myocardium in experimental models of ischemic myocardial injury and to correlate with $\alpha_v\beta_3$ integrin expression (*8,10*). In this study, we found consistently increased uptake of [^{68}Ga]Ga-NODAGA-RGD in the ischemic AAR at less than 14 d after AMI, a finding that is in line with previous studies showing accumulation of RGD-based tracers as early as 3 d after ischemic myocardial injury and then a peak at 1–3 wk (*6*). Uptake of [^{68}Ga]Ga-NODAGA-RGD was sometimes also observed adjacent to the AAR, as is consistent with previous evidence showing uptake of RGD-based tracers extending into the periinfarct zone (*12,21*). In contrast to AMI, accumulation of RGD-based tracers was not found in patients with chronic coronary total occlusion (*12*) or old myocardial infarction (*11,12,21*).

We found that the highest segmental uptake of [^{68}Ga]Ga-NODAGA-RGD (SUV_{max}) was 1.43-fold higher than the SUV_{mean} in the remote myocardium, which is similar to previous studies using different RGD-based tracers (1.34–2.33) (*11–13*). Using a rat model of AMI, we previously found that measurement of SUV using static images showed comparable results to kinetic modeling of the distribution volume of [^{68}Ga]Ga-DOTA-RGD uptake, thereby simplifying in vivo analysis (*9*). We also measured [^{68}Ga]Ga-NODAGA-RGD uptake corrected for both MBF and perfusable tissue fraction (indexed SUV_{max}) to account for reduced MBF and reduced distribution volume due to loss of viable tissue (*22*). Developments in scanner technology and motion correction algorithms may further facilitate quantification of the [^{68}Ga]Ga-NODAGA-RGD signal.

TABLE 3
[^{68}Ga]Ga-NODAGA-RGD and [^{15}O]O-Water PET Data

Parameter	AAR	Remote area	*P*
[^{68}Ga]Ga-NODAGA-RGD SUV_{max}	0.727 ± 0.16	0.529 ± 0.14	<0.001
[^{68}Ga]Ga-NODAGA-RGD SUV_{mean}	0.652 ± 0.15	0.511 ± 0.11	<0.001
Mean MBF	0.732 ± 0.23	0.827 ± 0.23	<0.001
Indexed [^{68}Ga]Ga-NODAGA-RGD SUV_{max}	1.263 ± 0.64	0.789 ± 0.24	<0.001

Data are mean ± SD.

Determinants of [^{68}Ga]Ga-NODAGA-RGD Uptake

Uptake of [^{68}Ga]Ga-NODAGA-RGD colocalized with injured myocardial areas based on reduced systolic LS on echocardiography and correlated with the degree of LS reduction after AMI. In a previous study, LS reduction was associated with the transmurality of myocardial injury according to late gadolinium enhancement on cardiac MRI (*17*). Thus, our findings are consistent with experimental (*10*) as well as clinical studies that found colocalization of RGD-based tracer uptake with resting myocardial perfusion defects (*11,13,21*), hypokinesia (*12*), and late gadolinium enhancement (*12,21*). In line with previous studies using other RGD-based tracers (*12,21*), [^{68}Ga]Ga-NODAGA-RGD uptake was also present in the periinfarct border zone and in 5 patients without wall motion abnormality at the time of the PET scan, indicating that it is a sensitive marker of recent ischemic myocardial injury.

Myocardial infarct size determined by peak troponin was not an independent predictor of the indexed [^{68}Ga]Ga-NODAGA-RGD SUV_{max}, indicating that $\alpha_v\beta_3$ integrin expression is also dependent on factors other than the extent of myocardial injury. Our finding is consistent with no association between uptake of another RGD-based tracer and infarct size quantified by cardiac MRI early after AMI (*12*). However, other studies reported correlations between uptake of other RGD-based tracers and infarct size late after AMI (31 ± 14 d and 8 wk) (*13,21*). Furthermore, an inverse relationship between ^{18}F-galacto-RGD uptake and resting MBF has been reported (*13*). In our study, uptake of [^{68}Ga]Ga-NODAGA-RGD did not correlate with overall MBF in the AAR consisting of a mixture of injured and noninjured myocardium but was associated with preserved MBF in the periinfarct border zone.

A novel finding in the present study is that in addition to LV dysfunction in the AAR, reduced LVEF, impaired GLS, and high NT-proBNP were independent predictors of [^{68}Ga]Ga-NODAGA-RGD uptake. These findings are consistent with the key roles of hemodynamic stress and pressure overload in modifying the responses of different cell types toward maintenance of cardiac function after injury (*1*). Taken together, our results are consistent with the increased expression of $\alpha_v\beta_3$ integrin after ischemic myocardial injury and with the intensity of [^{68}Ga]Ga-NODAGA-RGD

TABLE 4
Predictors of [^{68}Ga]Ga-NODAGA-RGD Uptake in AAR After AMI

	Univariable analysis			Multivariable analysis		
Predictor	B coefficient	R coefficient	*P*	B coefficient	R coefficient	*P*
SUV_{max}						
Age	0.001 (−0.005–0.008)	0.077	0.6			
Peak troponin T	0.002 (0.001–0.003)	0.603	<0.001			
Peak NT-proBNP	0.001 (0.001–0.002)	0.605	<0.001	0.001 (0.001–0.002)	0.605	<0.001
Baseline LVEF	−0.008 (−0.016–0.000)	−0.348	0.055			
Baseline GLS	0.016 (0.004–0.028)	0.447	0.01			
AAR LS	0.010 (0.001–0.020)	0.394	0.02			
Indexed SUV_{max}						
Age	−0.002 (−0.030–0.026)	−0.033	0.8			
Peak troponin T	0.011 (0.008–0.015)	0.765	<0.001	0.008 (0.005–0.012)	0.542	<0.001
Peak NT-proBNP	0.004 (0.002–0.007)	0.561	0.002			
Baseline LVEF	−0.067 (−0.093–0.041)	−0.701	<0.001	−0.045 (−0.067–0.023)	−0.476	<0.001
Baseline GLS	0.106 (0.069–0.143)	0.741	<0.001	0.061 (0.014–0.109)	0.422	0.01
AAR LS	0.071 (0.040–0.101)	0.668	<0.001	0.035 (−0.002–0.071)	0.315	0.059

Data in parentheses are 95% CI. Covariates in multivariable model were peak troponin T, peak NT-proBNP, and either LVEF, GLS, or AAR longitudinal strain. Peak troponin T is for 100-unit increment, and peak NT-proBNP is for 10-unit increment.

TABLE 5
Predictors of LV Function Improvement at Follow-up

Predictor	B coefficient	R coefficient	*P*
Improvement in LVEF*			
Age	0.004 (−0.001–0.009)	0.272	0.1
Peak troponin T	0.000 (−0.001–0.001)	−0.071	0.7
Peak NT-proBNP	0.000 (−0.001–0.000)	−0.228	0.2
SUV_{max} in AAR	0.004 (−0.309–0.316)	0.005	0.9
Indexed SUV_{max} in AAR	0.047 (−0.031–0.125)	0.233	0.2
Baseline GLS	0.007 (−0.003–0.018)	0.260	0.1
Improvement in GLS*			
Age	0.010 (−0.006–0.025)	0.232	0.2
Peak troponin T	0.004 (0.002–0.007)	0.519	0.003
Peak NT-proBNP	0.002 (0.000–0.004)	0.435	0.02
SUV_{max} in AAR	0.666 (−0.190–1.523)	0.288	0.1
Indexed SUV_{max} in AAR	0.319 (0.128–0.510)	0.550	0.002
Baseline LVEF	−0.023 (−0.042–0.004)	−0.423	0.02

*Adjusted for baseline. Peak troponin T is for 100-unit increment and peak NT-proBNP is for 10-unit increment.
Data in parentheses are 95% CI.

uptake reflecting both regional and global LV dysfunction, as well as increased LV filling pressure. Since global LV remodeling and dysfunction are robust risk factors for heart failure and mortality after AMI (*1,23*), our findings indicate that [^{68}Ga]Ga-NODAGA-RGD uptake is a potentially relevant prognostic biomarker.

Uptake of [^{68}Ga]Ga-NODAGA-RGD and Ventricular Function After AMI

Despite improvements in acute management, AMI remains one of the most important causes of chronic heart failure (*1*). Early detection of myocardial responses to injury could provide the opportunity for targeting and monitoring therapies, such as therapeutic angiogenesis, to attenuate adverse LV remodeling and systolic dysfunction (*1,3,24*). A novel finding of our study is that increased indexed [^{68}Ga]Ga-NODAGA-RGD SUV_{max} was associated with improvement in global LV function at follow-up, independently of peak troponin T, elevated NT-proBNP, and impaired LVEF. Our finding is in line with preclinical and clinical data suggesting that increased $\alpha_v\beta_3$ integrin expression after AMI predicts improvement of regional LV function (*12*) and the absence of adverse remodeling (*7,21*). However, in our study, [^{68}Ga]Ga-NODAGA-RGD was not directly associated with the functional outcome of the myocardium in the AAR. This finding may be explained by the functional outcome's being dependent mainly on the extent of irreversible myocardial injury whereas the repair processes affect viable surrounding myocardium, impacting adverse LV remodeling and global LV function (*1*).

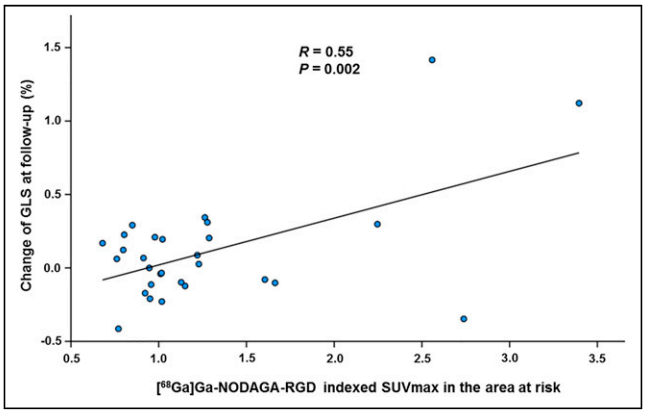

FIGURE 4. At follow-up, [^{68}Ga]Ga-NODAGA-RGD SUV_{max} in AAR predicted improvement of global longitudinal strain.

Limitations of Study

We studied patients within 3–14 d after AMI on the basis of experimental studies indicating that $\alpha_v\beta_3$ integrin expression peaks at 1–3 wk after AMI (*6*). There was no difference in the uptake of [^{68}Ga]Ga-NODAGA-RGD between patients scanned before versus after 7 d after AMI, indicating relatively stable uptake at this time. Our ability to detect associations between the uptake of [^{68}Ga]Ga-NODAGA-RGD and changes in LV structure and function may have been limited by the modest degree of changes and limited number of patients with significant LV remodeling despite a relatively long time from symptom onset to revascularization. Furthermore, cardiac MRI could have provided more precise quantification of cardiac structure and function than echocardiography despite a standardized, predefined protocol. The predictive value of endothelial progenitor cells, proposed to contribute to angiogenesis, versus [^{68}Ga]Ga-NODAGA-RGD PET for functional recovery remains to be explored in future studies. Although a formal power calculation was not feasible, the sample size of 30 patients would be sufficient—on the basis of a previous experimental study (*7*)—to detect differences in tracer uptake between those with and without significant remodeling.

CONCLUSION

In patients with AMI, [^{68}Ga]Ga-NODAGA-RGD uptake was increased in the ischemic AAR, correlating with the extent of myocardial injury, global and regional LV dysfunction, and LV filling pressure. Furthermore, [^{68}Ga]Ga-NODAGA-RGD uptake predicted global LV function improvement at the midterm follow-up. These results suggest that targeted imaging of $\alpha_v\beta_3$ integrin is a potential approach to evaluate myocardial injury responses after AMI.

DISCLOSURE

Financial support was received from grants from the Academy of Finland, the Finnish Foundation for Cardiovascular Research, and State Research Funding of Turku University Hospital. Antti Saraste discloses speaker or consultancy fees from Amgen, Abbott, Astra Zeneca, Bayer, Novartis, and Pfizer outside the submitted work. Juhani Knuuti discloses consultancy fees from GE Healthcare and speaker fees from GE Healthcare, Bayer, Lundbeck, Boehringer Ingelheim, Pfizer, Siemens, and Merck outside the submitted work. No other potential conflict of interest relevant to this article was reported.

KEY POINTS

QUESTION: We prospectively evaluated determinants of [^{68}Ga]Ga-NODAGA-RGD uptake, a PET tracer targeting $\alpha_v\beta_3$ integrin, after myocardial infarction and its associations with LV function at follow-up.

PERTINENT FINDINGS: In 31 patients with AMI, [^{68}Ga]Ga-NODAGA-RGD uptake increased in the ischemic AAR early after myocardial infarction, and this increase was associated with the severity of myocardial injury, LV systolic dysfunction, and increased LV filling pressure. Increased [^{68}Ga]Ga-NODAGA-RGD uptake predicted improvement of global LV function.

IMPLICATIONS FOR PATIENT CARE: Uptake of [^{68}Ga]Ga-NODAGA-RGD is a potentially relevant prognostic biomarker in AMI and might identify patients who could benefit from therapeutic interventions aimed at improving myocardial repair after AMI.

REFERENCES

1. Frantz S, Hundertmark MJ, Schulz-Menger J, Bengel FM, Bauersachs J. Left ventricular remodelling post-myocardial infarction: pathophysiology, imaging, and novel therapies. *Eur Heart J.* 2022;43:2549–2561.
2. Wu X, Reboll MR, Korf-Klingebiel M, Wollert KC. Angiogenesis after acute myocardial infarction. *Cardiovasc Res.* 2021;117:1257–1273.
3. Simons M, Alitalo K, Annex BH, et al. State-of-the-art methods for evaluation of angiogenesis and tissue vascularization: a scientific statement from the American Heart Association. *Circ Res.* 2015;116:e99–e132.
4. Sun M, Opavsky MA, Stewart DJ, et al. Temporal response and localization of integrins beta1 and beta3 in the heart after myocardial infarction: regulation by cytokines. *Circulation.* 2003;107:1046–1052.
5. Meoli DF, Sadeghi MM, Krassilnikova S, et al. Noninvasive imaging of myocardial angiogenesis following experimental myocardial infarction. *J Clin Invest.* 2004;113:1684–1691.
6. Higuchi T, Bengel FM, Seidl S, et al. Assessment of αvβ3 integrin expression after myocardial infarction by positron emission tomography. *Cardiovasc Res.* 2008;78:395–403.
7. Sherif HM, Saraste A, Nekolla SG, et al. Molecular imaging of early αvβ3 integrin expression predicts long-term left-ventricle remodeling after myocardial infarction in rats. *J Nucl Med.* 2012;53:318–323.
8. Laitinen I, Notni J, Pohle K, et al. Comparison of cyclic RGD peptides for αvβ3 integrin detection in a rat model of myocardial infarction. *EJNMMI Res.* 2013;3:38.
9. Kiugel M, Dijkgraaf I, Kytö V, et al. Dimeric [^{68}Ga]DOTA-RGD peptide targeting αvβ 3 integrin reveals extracellular matrix alterations after myocardial infarction. *Mol Imaging Biol.* 2014;16:793–801.
10. Grönman M, Tarkia M, Kiviniemi T, et al. Imaging of alphavbeta3 integrin expression in experimental myocardial ischemia with [^{68}Ga]NODAGA-RGD positron emission tomography. *J Transl Med.* 2017;15:144.
11. Sun Y, Zeng Y, Zhu Y, et al. Application of ^{68}Ga-PRGD2 PET/CT for αvβ3-integrin imaging of myocardial infarction and stroke. *Theranostics.* 2014;4:778–786.
12. Jenkins WS, Vesey AT, Stirrat C, et al. Cardiac αVβ3 integrin expression following acute myocardial infarction in humans. *Heart.* 2017;103:607–615.
13. Makowski MR, Rischpler C, Ebersberger U, et al. Multiparametric PET and MRI of myocardial damage after myocardial infarction: correlation of integrin αvβ3 expression and myocardial blood flow. *Eur J Nucl Med Mol Imaging.* 2021;48:1070–1080.
14. Gnesin S, Mitsakis P, Cicone F, et al. First in-human radiation dosimetry of ^{68}Ga-NODAGA-RGDyK. *EJNMMI Res.* 2017;7:43.
15. Lehtonen E, Teuho J, Koskinen J, et al. A respiratory motion estimation method based on inertial measurement units for gated positron emission tomography. *Sensors (Basel).* 2021;21:3983.
16. Grönman M, Tarkia M, Stark C, et al. Assessment of myocardial viability with [^{15}O]water PET: a validation study in experimental myocardial infarction. *J Nucl Cardiol.* 2021;28:1271–1280.
17. Rost C, Rost MC, Breithardt OA, et al. Relation of functional echocardiographic parameters to infarct scar transmurality by magnetic resonance imaging. *J Am Soc Echocardiogr.* 2014;27:767–774.
18. Antonov AS, Antonova GN, Munn DH, et al. αVβ3 integrin regulates macrophage inflammatory responses via PI3 kinase/Akt-dependent NF-κB activation. *J Cell Physiol.* 2011;226:469–476.
19. Sarrazy V, Koehler A, Chow ML, et al. Integrins αvβ5 and αvβ3 promote latent TGF-β1 activation by human cardiac fibroblast contraction. *Cardiovasc Res.* 2014;102:407–417.
20. van den Borne SW, Isobe S, Verjans JW, et al. Molecular imaging of interstitial alterations in remodeling myocardium after myocardial infarction. *J Am Coll Cardiol.* 2008;52:2017–2028.
21. Verjans J, Wolters S, Laufer W, et al. Early molecular imaging of interstitial changes in patients after myocardial infarction: comparison with delayed contrast-enhanced magnetic resonance imaging. *J Nucl Cardiol.* 2010;17:1065–1072.
22. MacAskill MG, Stadulyte A, Williams L, et al. Quantification of macrophage-driven inflammation during myocardial infarction with ^{18}F-LW223, a novel TSPO radiotracer with binding independent of the rs6971 human polymorphism. *J Nucl Med.* 2021;62:536–544.
23. Konstam MA, Kramer DG, Patel AR, Maron MS, Udelson JE. Left ventricular remodeling in heart failure: current concepts in clinical significance and assessment. *JACC Cardiovasc Imaging.* 2011;4:98–108.
24. Huang CC, Wei HJ, Lin KJ, et al. Multimodality noninvasive imaging for assessing therapeutic effects of exogenously transplanted cell aggregates capable of angiogenesis on acute myocardial infarction. *Biomaterials.* 2015;73:12–22.